

Chapter 4

The 2-fold d -Al-Ni-Co Surfaces

The high symmetry surfaces of a decagonal quasicrystal include the 10-fold and two inequivalent 2-fold surfaces. The 10-fold axis is along the periodic direction, while two inequivalent sets of 2-fold axes exist perpendicular to the 10-fold axis. These 2-fold axes appear alternately at 18° yielding a decagonal symmetry.

To introduce the surfaces, the bulk decagonal basis vectors shown in Figure 1.7 are reillustrated in Figure 4.1. The 10-fold axis runs along $[00001]$, which is perpendicular to the plane of paper. The two inequivalent sets of 2-fold axes can be represented by $[10000]$ and $[001\bar{1}0]$. The high symmetry directions of the (10000) surface are thus the periodic $[00001]$ and the quasiperiodic $[001\bar{1}0]$. Similarly, the high symmetry directions of the $(001\bar{1}0)$ surface are the periodic $[00001]$ and the quasiperiodic $[10000]$ ones. In this chapter investigations of the 2-fold d -Al_{71.8}Ni_{14.8}Co_{13.4}(10000) surface by SPA-LEED and HAS and the 2-fold d -Al_{71.8}Ni_{14.8}Co_{13.4}(001 $\bar{1}$ 0) surface by HAS are presented.

4.1 The 2-fold d -Al-Ni-Co(10000) Surface

4.1.1 Spot Profile Analyzing Low Energy Electron Diffraction

A large single grain d -Al_{71.8}Ni_{14.8}Co_{13.4} sample was cut along the (10000) plane. The surface was mechanically polished and transferred into the UHV chamber (base pressure 1×10^{-10} mbar). The surface was cleaned by repeated sputtering (Ne⁺ of 1-3 kV, 4-10 μ A, for 20-30 minutes)

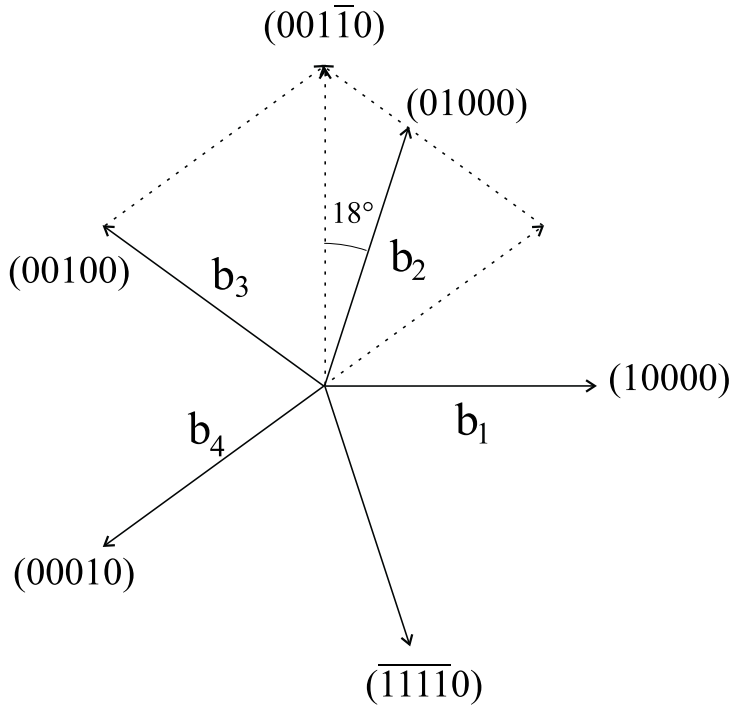


Figure 4.1: Reillustration of bulk decagonal basis vectors shown in Figure 1.7. The two inequivalent sets of 2-fold axes, represented by $[10000]$ and $[001\bar{1}0]$ appear alternately at 18° .

and annealing cycles (600-650 °C).

SPA-LEED images of the clean surface recorded at different electron energies are shown in Figure 4.2. The SPA-LEED images display sharp diffraction spots revealing a perfect long range order of the surface. The sharpness of spots is comparable to that of diffraction spots observed in the 10-fold *d*-Al_{71.8}Ni_{14.8}Co_{13.4} surface (Section 3.1).

The horizontal and vertical in the images are the periodic $[00001]$ and the quasiperiodic $[001\bar{1}0]$ direction, respectively. The density of spots along the quasiperiodic direction is very high (average 5 spots per \AA^{-1}), which is not unusual for quasicrystals. The distribution of the diffraction spots along the $[001\bar{1}0]$ -azimuth is shown by line scans in Figure 4.3. The peak positions are related by the golden mean reflecting a perfect quasicrystalline order in the surface region. The peak positions can be obtained by $\Delta k_{\parallel} = k_0(m + n\tau)$, with $k_0 = 0.60 \text{ \AA}^{-1}$ and (m, n) integers. The values of Δk_{\parallel} and (m, n) of each peak are listed in Table 4.1.

The observed peak positions are identical to the surface projection of the bulk reciprocal lattice structure. As introduced in Section 3.1, the bulk reciprocal vectors of *d*-Al_{71.8}Ni_{14.8}Co_{13.4} are $\mathbf{b}_j = 1.02(\cos \frac{2\pi j}{5}, \sin \frac{2\pi j}{5}, 0) \text{ \AA}^{-1}$ ($j = 1, \dots, 4$) and $\mathbf{b}_5 = 0.78(0, 0, 1) \text{ \AA}^{-1}$ (Figure 3.1), where \mathbf{b}_j ($j = 1, \dots, 4$) are within the quasiperiodic planes and \mathbf{b}_5 is along the periodic direction. The projection of \mathbf{b}_j ($j = 1, \dots, 4$) onto the quasicrystalline $[001\bar{1}0]$ -direction yields $P_{[001\bar{1}0]}(\mathbf{b}_1) = 0$,

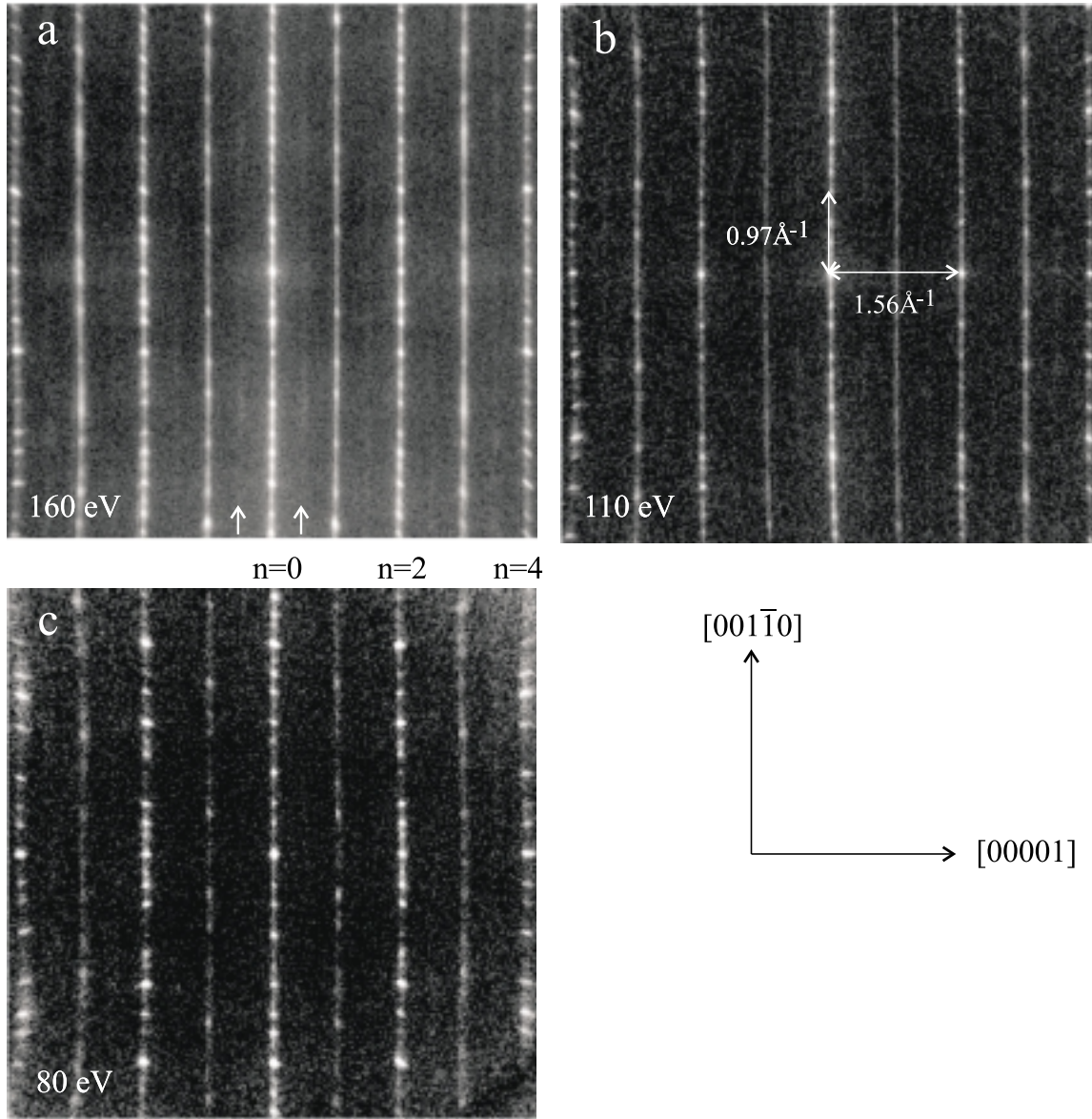


Figure 4.2: SPA-LEED images of the 2-fold d -Al_{71.8}Ni_{14.8}Co_{13.4}(10000) surface taken at 160 eV (a), 110 eV (b), and 80 eV (c) electron energy displaying a periodic ordering along [00001] and quasiperiodic ordering along [001̄10].

$P_{[001\bar{1}0]}(\mathbf{b}_2) = b \sin \frac{2\pi}{5} = b\tau \sin \frac{\pi}{5}$, $P_{[001\bar{1}0]}(\mathbf{b}_3) = b \sin \frac{\pi}{5}$, and $P_{[001\bar{1}0]}(\mathbf{b}_4) = -b \sin \frac{\pi}{5}$ (refer to Figure 4.4). The projection of any arbitrary vector in the quasicrystalline plane therefore results in $P_{[001\bar{1}0]}(\sum_{j=1}^4 n_j \mathbf{b}_j) = b \sin(\frac{\pi}{5})(m + n\tau) = k_0(m + n\tau)$, which agrees perfectly with the observed diffraction pattern.

The k -vectors of the vertical columns of diffraction spots are nb_5 , with $n = 0, \pm 1, \pm 2, \pm 3,$

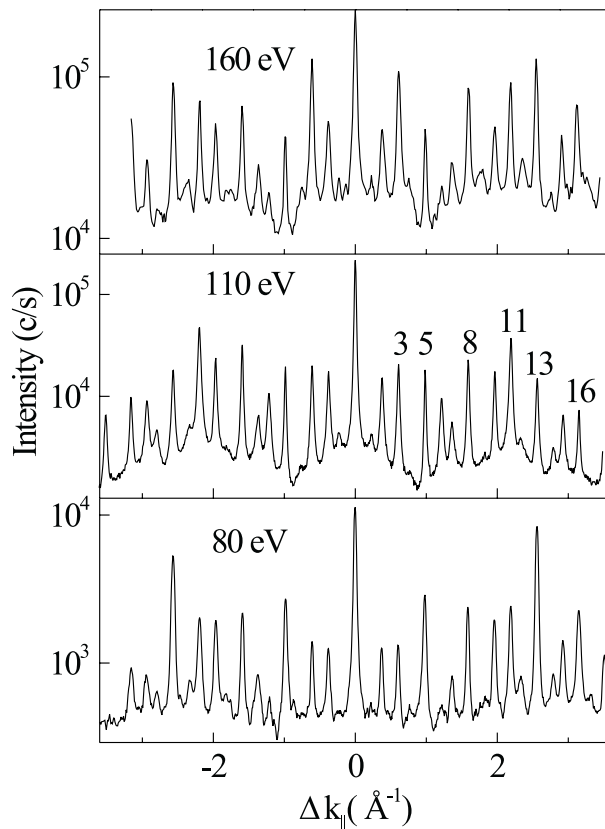


Figure 4.3: Line scans along the quasicrystalline $[001\bar{1}0]$ direction. (Intensity in logarithmic scale).

and ± 4 , and $b_5 = 0.78 \text{ \AA}^{-1}$. This corresponds to an 8 \AA periodicity along the periodic $[00001]$ direction reflecting a doubling of the minimum periodicity of the decagonal system given by two layers with an interlayer distance of 2.04 \AA . The observed 8 \AA periodicity is in agreement with the bulk reciprocal lattice structure [64, 80].

In addition to the 8 \AA periodicity, very weak streaks (shown by arrows in Figure 4.2) corresponding to a 16 \AA periodicity also appear in the SPA-LEED images (see also in line scan in Figure 4.9). So far, no evidence of a 16 \AA periodicity is reported in the *d*-Al-Ni-Co system. As revealed by He diffraction, the topmost layer of the surface also preserves the weak 16 \AA periodicity (see Section 4.1.2). Furthermore, He diffraction of the other inequivalent 2-fold surface of *d*-Al_{71.8}Ni_{14.8}Co_{13.4} also shows a weak 16 \AA periodicity. Since the 16 \AA periodicity is observed in both inequivalent 2-fold surfaces and the intensity of the 16 \AA peaks associated with the topmost layer (HAS) does not significantly differ from that resulting from the few mono-

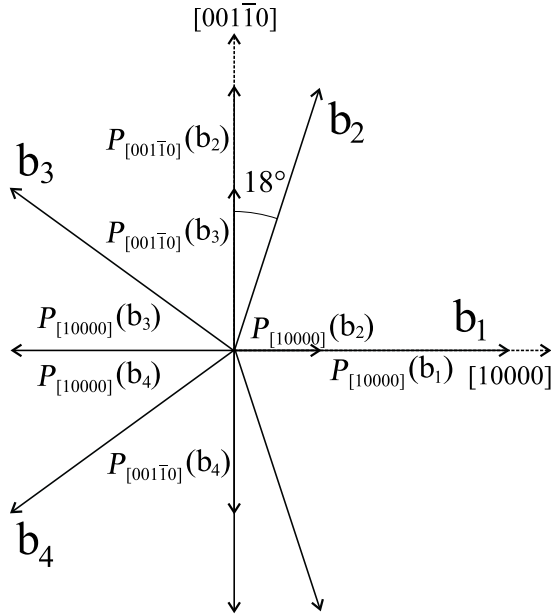


Figure 4.4: The projection of the in-plane bulk decagonal basis vectors \mathbf{b}_j ($j = 1, \dots, 4$) onto $[10000]$ and $[001\bar{1}0]$, the two inequivalent 2-fold axes.

layers (SPA-LEED), the new periodicity is most likely a bulk feature and not due to a surface reconstruction.

The SPA-LEED images display an identical distribution of the spots (both position and intensity) in all even columns. The width of the spots along the periodic and quasiperiodic directions is isotropic within the error of SPA-LEED electron optics. The distribution of the spots on the odd columns is qualitatively different compared to that on the even columns. In contrast to the isotropic width of the spots in the even columns, the spots in the odd columns are broadened along the quasiperiodic direction, while they exhibit only instrumental broadening along the periodic direction. The FWHM of the spots along the quasiperiodic direction is about 0.08 \AA^{-1} , which is 3-4 times larger than that along the periodic direction. This indicates a short range lateral correlation of atoms in the layers corresponding to the 8 \AA periodicity.

In addition to these structural investigations, the surface morphology was studied. Information on vertical roughness of surfaces such as step distribution and orientation of facets can be achieved by measuring LEED intensities as a function of vertical scattering vector k_{\perp} . The intensity profiles of the measured diffraction spots reflect the surface morphology [120].

Figure 4.5 shows the measured LEED intensity $I(k_{\parallel}, k_{\perp})$ in gray scale representation with k_{\perp} along $[10000]$ and k_{\parallel} along $[001\bar{1}0]$. The vertical rods (m, n) present the intensity variations of diffraction spots at $\Delta k_{\parallel} = k_0(m + n\tau)$, with $k_0 = 0.60 \text{ \AA}^{-1}$ and $(m, n) = (0, 0), \pm(2, \bar{1}), \pm(\bar{1}, 1)$,

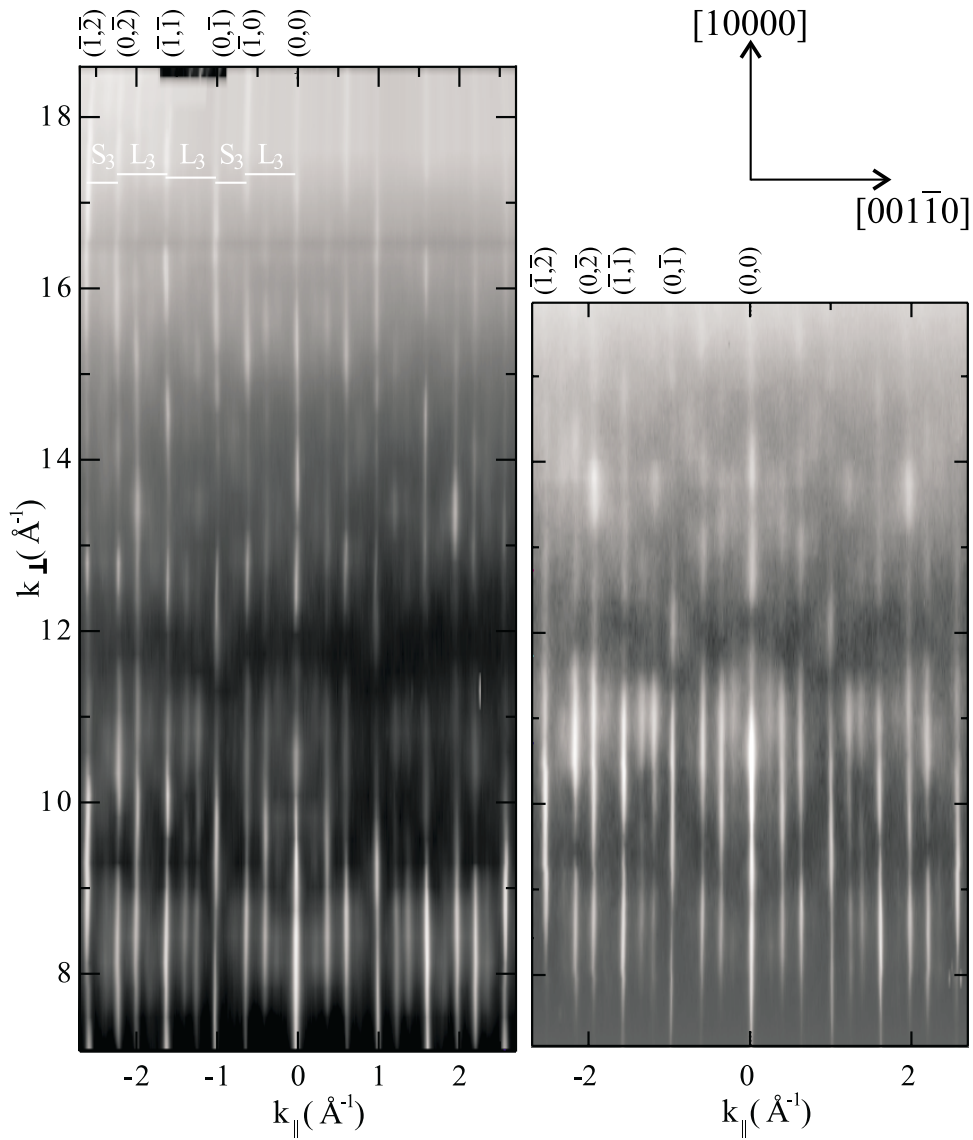


Figure 4.5: A gray scale plot of LEED intensity $I(k_{\parallel}, k_{\perp})$ with k_{\perp} along $[10000]$ (vertical) and k_{\parallel} along $[001\bar{1}0]$ (horizontal). Left: 0^{th} order spots (spots on the 0^{th} column of SPA-LEED image, Figure 4.2) and right: 2^{nd} order spots (spots on the 2^{nd} column).

$\pm(1,0)$, $\pm(2,\bar{2})$, $\pm(0,1)$, $\pm(2,0)$, $\pm(1,\bar{2})$, $\pm(1,1)$, $\pm(3,0)$, $\pm(0,2)$, $\pm(2,1)$, $\pm(4,0)$, and $\pm(1,2)$. Hence, the rods are separated by distances forming a sequence LSLSLLSLLSLS. The diffraction intensities are observable for a large electron energy range, revealing a highly ordered structure up to a significant depth from the topmost surface layer. The 0^{th} order spots (spots on the 0^{th} column of the SPA-LEED image in Figure 4.2) are detectable with sufficient intensity from 50

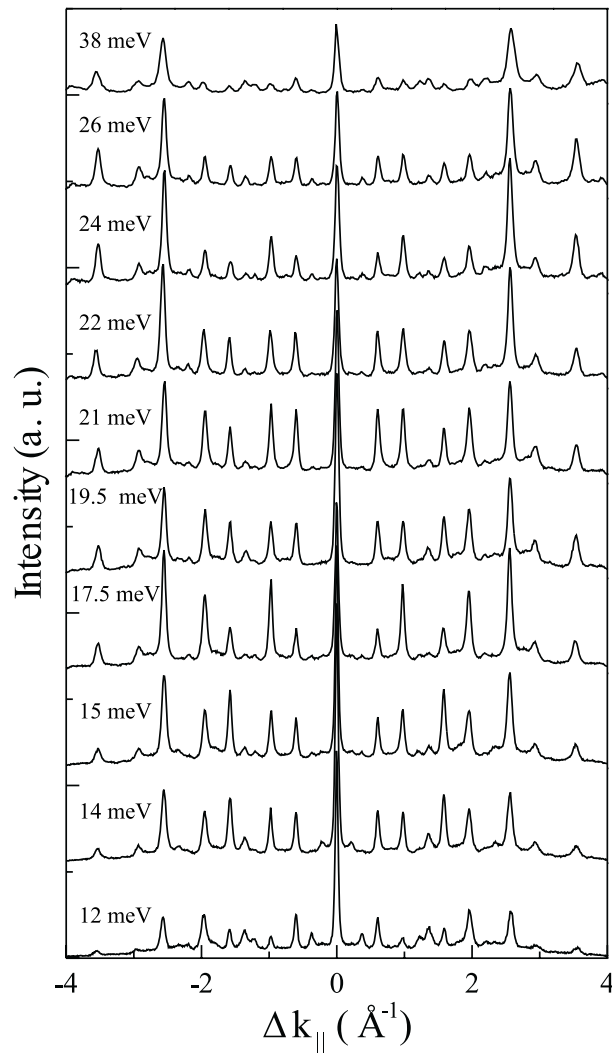


Figure 4.6: He diffraction along the quasicrystalline $[001\bar{1}0]$ direction at different beam energies from 12 meV to 38 meV.

of the higher order diffraction peaks decreases. For the strongest diffraction peak at 2.54 \AA^{-1} , the ratio varies from a factor of 5 to 1 for energy varying from 12 meV to 38 meV. The strong beam energy dependence is attributed to the high corrugation of the surface.

A comparison of He diffraction with SPA-LEED (Figure 4.7) reveals identical peak positions. The peaks which are strong in He diffraction also appear as stronger peaks in electron diffraction. However, two of the weak peaks represented by $\pm(2,1)$ and $\pm(2,2)$ are stronger in electron diffraction. The stronger spots of He diffraction thus break the Fibonacci sequence. They follow a sequence $L_3S_3L_3S_3L_3S_3L_3$, which has a repeating unit of L_3S_3 .

Peaks	(m, n)	$\Delta k_{\parallel}^i / \text{\AA}^{-1}$	δk		$\delta k'$		$\delta k''$		$(m, n)^*$	$(m, n)^\dagger$	$(m, n)^\ddagger$
1	$(2, \bar{1})$	0.23	0.23	L					$(\bar{1}, 1)$	$(1, 0)$	(0, 1)
2	$(\bar{1}, 1)$	0.37	0.14	S					$(1, 0)$	(0, 1)	(1, 1)
3	$(1, 0)$	0.60	0.23	L	0.60	L_3	0.60	L_3	(0, 1)	(1, 1)	(1, 2)
4	$(2, \bar{2})$	0.74	0.14	S					$(2, 0)$	$(0, 2)$	$(2, 2)$
5	(0, 1)	0.97	0.23	L	0.37	S_3	0.37	S_3	(1, 1)	(1, 2)	(2, 3)
6	$(2, 0)$	1.21	0.24	L					$(0, 2)$	$(2, 2)$	$(2, 4)$
7	$(1, \bar{2})$	1.34	0.13	S					$(2, 1)$	$(1, 3)$	$(3, 4)$
8	(1, 1)	1.57	0.23	L	0.60	L_3	0.60	L_3	(1, 2)	(2, 3)	(3, 5)
9	$(3, 0)$	1.80	0.23	L					$(0, 3)$	$(3, 3)$	$(3, 6)$
10	$(0, 2)$	1.94	0.14	S	0.37	S_3			$(2, 2)$	$(2, 4)$	$(4, 6)$
11^b	$(2, 1)$	2.17	0.13	L			0.60	L_3	$(1, 3)$	$(3, 4)$	$(4, 7)$
12	$(4, 0)$	2.40	0.13	S					$(0, 4)$	$(4, 4)$	$(4, 8)$
13	(1, 2)	2.54	0.24	L	0.60	L_3	0.37	S_3	(2, 3)	(3, 5)	(5, 8)
14	$(3, 1)$	2.77	0.23	L					$(1, 4)$	$(4, 5)$	$(5, 9)$
15	$(0, 3)$	2.91	0.14	S	0.37	S_3			$(3, 3)$	$(3, 6)$	$(6, 9)$
16^b	$(2, 2)$	3.14	0.23	L			0.60	L_3	$(2, 4)$	$(4, 6)$	$(6, 10)$
17	$(4, 1)$	3.37	0.23	S					$(1, 5)$	$(5, 6)$	$(6, 11)$
18	$(1, 3)$	3.51	0.14	L	0.37	L_3			$(3, 4)$	$(4, 7)$	$(7, 11)$
19 ^a	$(3, 2)$	3.74	0.23	L					$(2, 5)$	$(5, 7)$	$(7, 12)$
20 ^a	$(0, 4)$	3.88	0.14	S					$(4, 4)$	$(4, 8)$	$(8, 12)$
21 ^a	(2, 3)	4.11	0.23	L					(3, 5)	(5, 8)	(8, 13)
22 ^a	$(4, 2)$	4.34	0.23	L					$(2, 6)$	$(6, 8)$	so on
23 ^a	$(1, 4)$	4.49	0.15	S					$(4, 5)$	$(5, 9)$...

Table 4.1: The diffraction vectors of 2-fold d -Al_{71.8}Ni_{14.8}Co_{13.4}(10000) surface along the quasicrystalline $[001\bar{1}0]$ direction. δk : difference between the vectors of two successive peaks. $\delta k'$ ($\delta k''$): difference between the vectors of two successive strong peaks of He diffraction (electron diffraction). Diffraction vectors of strong peaks and the Fibonacci pairs are written in bold characters. (^adetected only in He diffraction, ^bappears as stronger spot only in electron diffraction. $(m, n)^*$, $(m, n)^\dagger$, and $(m, n)^\ddagger$ are values for $i = -1, -2$, and -3 , respectively).

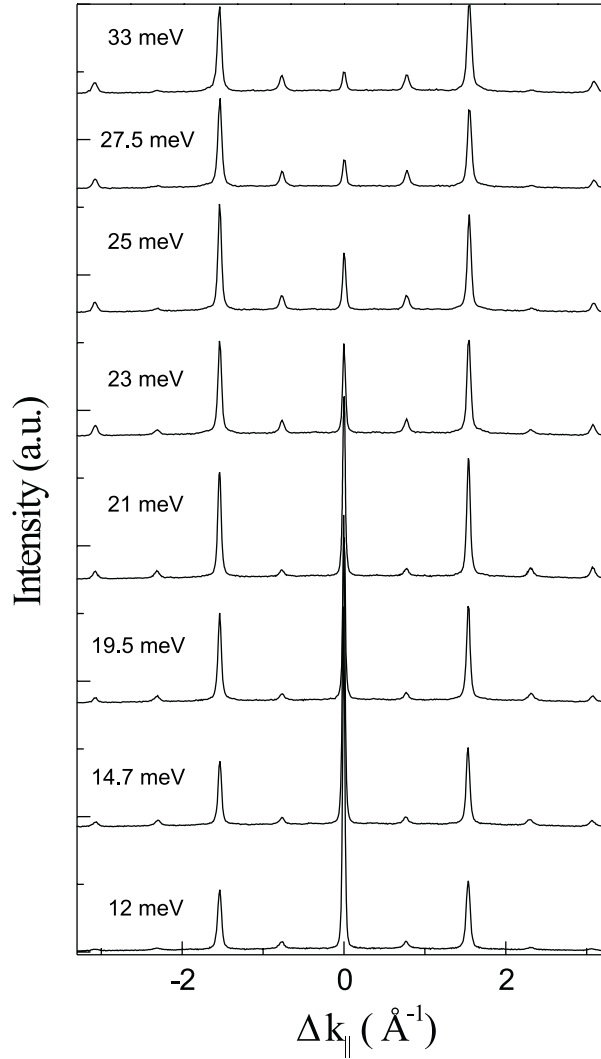


Figure 4.8: He diffraction along the periodic [00001] direction at different beam energies from 12 meV to 33 meV.

This property can be illustrated also by taking new basis vectors which are τ^i multiples of k_0 and k_1 , with i integers. The peak positions with respect to these new basis vectors can be obtained by $\Delta k_{||} = k_0 \tau^i (m + n\tau)$. The values of (m, n) for $i = -1, -2$, and -3 are given in Table 4.1. One can see many stronger peaks take the two successive Fibonacci numbers with respect to smaller basis vectors.

Helium diffraction along the periodic [00001] direction for different beam energies from 12 meV to 33 meV are shown in Figure 4.8. Intensity of diffraction peaks strongly depends on beam energy. With increasing beam energy, the intensity of the diffraction peaks increases with

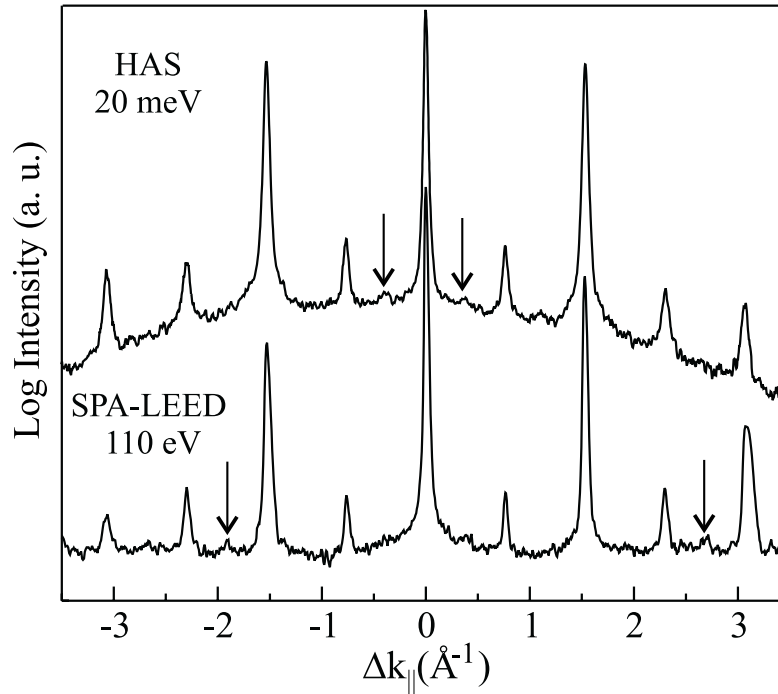


Figure 4.9: A comparison between HAS and SPA-LEED along the periodic [00001] direction (upper: He diffraction at 20 meV beam energy and lower: Electron diffraction at 110 eV electron energy). Weak peaks indicated by arrows correspond to a 16 Å periodicity.

respect to the specular intensity. The ratio of the specular intensity to the intensity of the peak at 1.56 \AA^{-1} varies from a factor of 5 to 0.25 for beam energy ranging from 12 meV to 33 meV.

A comparison of He diffraction with electron diffraction along the periodic [00001] direction is shown in Figure 4.9. Peak positions are identical at $\pm 0.39 \text{ \AA}^{-1}$, $\pm 0.78 \text{ \AA}^{-1}$, $\pm 1.16 \text{ \AA}^{-1}$, and $\pm 1.56 \text{ \AA}^{-1}$. The peaks at $\pm 0.78 \text{ \AA}^{-1}$ correspond to the main 8 Å periodicity, while the weak peaks at $\pm 0.39 \text{ \AA}^{-1}$ (indicated by arrows) to a 16 Å periodicity. The 16 Å periodic peaks are weak in both He and electron diffraction.

4.2 The 2-fold *d*-Al-Ni-Co(001 $\bar{1}$ 0) Surface

In this section, He diffraction from the 2-fold *d*-Al_{71.8}Ni_{14.8}Co_{13.4}(001 $\bar{1}$ 0) surface along the quasicrystalline [10000] direction is discussed. Diffraction along the periodic [00001] direction reveals the 8 Å bulk periodicity. The diffraction data are very similar to those observed along the periodic [00001] direction of the 2-fold *d*-Al_{71.8}Ni_{14.8}Co_{13.4}(10000) surface (Section 4.1.2) including

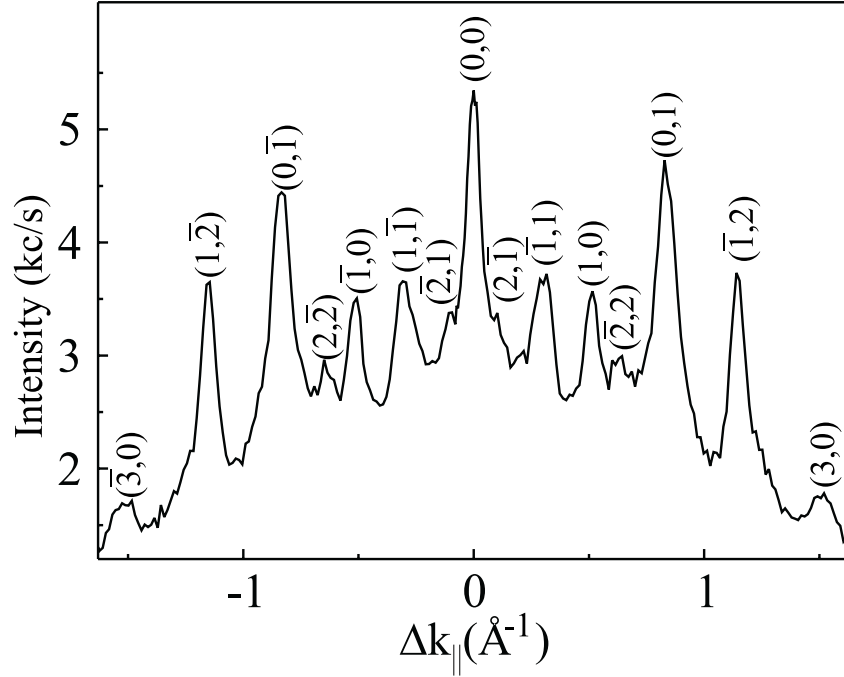


Figure 4.10: He diffraction spectrum from the 2-fold d -Al_{71.8}Ni_{14.8}Co_{13.4}(001 $\bar{1}$ 0) surface along the quasicrystalline [10000]-direction at 21 meV He atom kinetic energy. The peaks are at $\Delta k_{\parallel} = 0.51(m + n\tau) \text{ \AA}^{-1}$, with m and n integers. Values of m and n are shown above the peaks.

the extremely weak peaks corresponding to the 16 \AA periodicity.

Figure 4.10 shows He diffraction from the surface after several cycles of Ne⁺ sputtering (3 kV, 15-20 minutes, 6 μA) and annealing at 600-650 $^{\circ}\text{C}$. The surface was cleaned and its quality was monitored by the same procedures employed for the (10000) surface (Section 4.1.2). As can be seen in the spectrum, the intensity of the diffraction peaks is comparable to that of the specular direction, revealing a high corrugation of the topmost surface layer. A similar corrugation is observed on the 2-fold (10000) surface (Section 4.1.2). In contrast, the 10-fold surface has a very low corrugation (Section 3.2).

The peaks at 0.19 \AA^{-1} , 0.31 \AA^{-1} , 0.51 \AA^{-1} , 0.63 \AA^{-1} , 0.83 \AA^{-1} , 1.14 \AA^{-1} , and 1.53 \AA^{-1} correspond to $\Delta k_{\parallel} = (k_0/\chi)(m + n\tau)$, $k_0/\chi = 0.51 \text{ \AA}^{-1}$, with $(m,n) = (2, \bar{1})$, $(\bar{1}, 1)$, $(1,0)$, $(\bar{2}, 2)$, $(0,1)$, $(\bar{1}, 2)$, and $(3,0)$, respectively. These peak positions can be compared to the surface projection of the bulk reciprocal lattice structure. Projection of the bulk reciprocal vectors \mathbf{b}_j ($j = 1, \dots, 4$) onto the quasicrystalline [10000]-direction of the (001 $\bar{1}$ 0)-surface yields $P_{[10000]}(\mathbf{b}_1) = b$, $P_{[10000]}(\mathbf{b}_2) = b \cos \frac{2\pi}{5} = b(\tau - 1)/2$ and $P_{[10000]}(\mathbf{b}_3) = P_{[10000]}(\mathbf{b}_4) = -b \cos \frac{\pi}{5} = -b\tau/2$ (refer

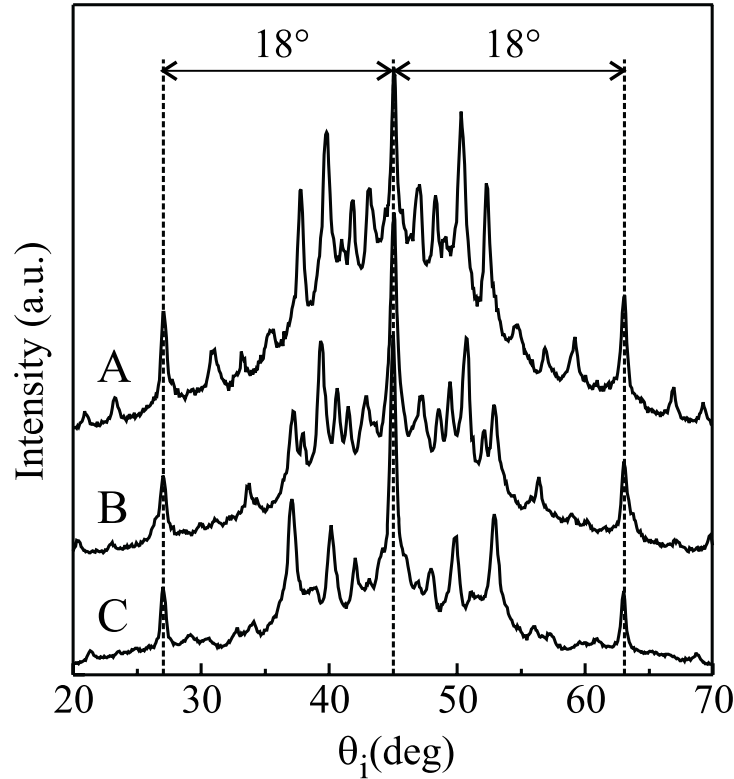


Figure 4.11: Angular distribution of He diffraction along the quasicrystalline direction for different energies (A: 21.5 meV, B: 18.2 meV and C: 9.5 meV). The peaks at $\theta_i = 27^\circ$ and 63° are reflections from the facets inclined by 18° .

to Figure 4.4). The projection of any arbitrary vector in the quasicrystalline plane therefore results in $P_{[10000]}(\sum_{j=1}^4 n_j \mathbf{b}_j) = b(m + n\tau)/2 = (k_0/\chi)(m + n\tau)$ in perfect agreement with the observed diffraction pattern.

Figure 4.11 shows the angular distribution in He diffraction along the quasicrystalline direction at different beam energies. All diffraction peaks except those at $\theta_i = 27^\circ$ and 63° shift with incident beam energy as expected. The fixed peaks (marked by dotted lines) are 18° off from the specular peak of the original or cut surface and are identified as the specular peaks of facets inclined by 18° with respect to the original surface. These facets have (10000)-equivalent surfaces, as (10000) and (001 $\bar{1}$ 0) form an angle of 90° , which is equal to 18° plus 72° , the rotation angle of the 5-fold symmetry (see Figure 4.1).

Expected diffraction peak positions from the facets based on the bulk structure can be obtained by a projection of the basis vectors onto the quasiperiodic [001 $\bar{1}$ 0]-direction of the

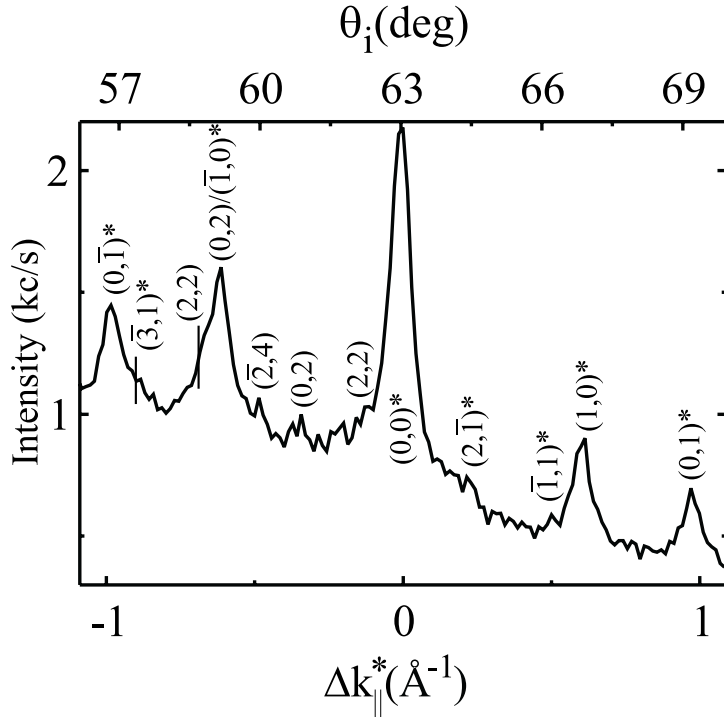


Figure 4.12: Region around $\theta_i = 63^\circ$ of the top spectrum in Figure 4.11. (m, n) and $(m, n)^*$ label diffraction from the original surface and facets, respectively. Δk_{\parallel} is the parallel momentum transfer in scattering from the facets

(10000)-surface. The projections yield $P_{[001\bar{1}0]}(\mathbf{b}_1) = 0$, $P_{[001\bar{1}0]}(\mathbf{b}_2) = b \sin \frac{2\pi}{5} = b\tau \sin \frac{\pi}{5}$, and $P_{[001\bar{1}0]}(\mathbf{b}_3) = P_{[001\bar{1}0]}(\mathbf{b}_4) = -b \sin \frac{\pi}{5}$ (refer to Figure 4.4). Therefore, the diffraction peaks from the facets are expected at $\Delta k_{\parallel}^* = P_{[001\bar{1}0]}(\sum_{j=1}^4 n_j \mathbf{b}_j) = b \sin \frac{\pi}{5} (m + n\tau) = k_0 (m + n\tau)$, with $k_0 = 0.60 \text{ \AA}^{-1}$. The parallel momentum transfer in scattering from the facets can be calculated by $\Delta k_{\parallel}^* = \sqrt{2mE_i/\hbar^2} (\cos \theta_i^* - \sin \theta_i^*)$, where θ_i^* is the angle of incident beam with respect to the facet normal and given by $\theta_i^* = \theta_i \pm 18^\circ$. Figure 4.12 is a close up view of the top spectrum in Figure 4.11 around the facet specular. The peaks labeled with $(m, n)^*$ are found at the positions expected from the $P_{[001\bar{1}0]}$ -projected basis vectors, hence identified as diffraction peaks from the facets.

In fact, the diffraction peaks from the facets appear at the identical position of peaks observed in the 2-fold d -Al_{71.8}Ni_{14.8}Co_{13.4}(10000) surface along the quasiperiodic $[001\bar{1}0]$ direction, which is demonstrated by comparing the diffraction from the facets and the 2-fold (10000) surface in Figure 4.13. In contrast to the spectra from the 2-fold (10000) surface, the intensities of facet diffraction peaks are not symmetric on the left and the right of the specular. This arises from the alignment of sample with respect to the surface normal, not to facet normal.

In addition to the comparison of angular distribution in diffraction from the facet planes

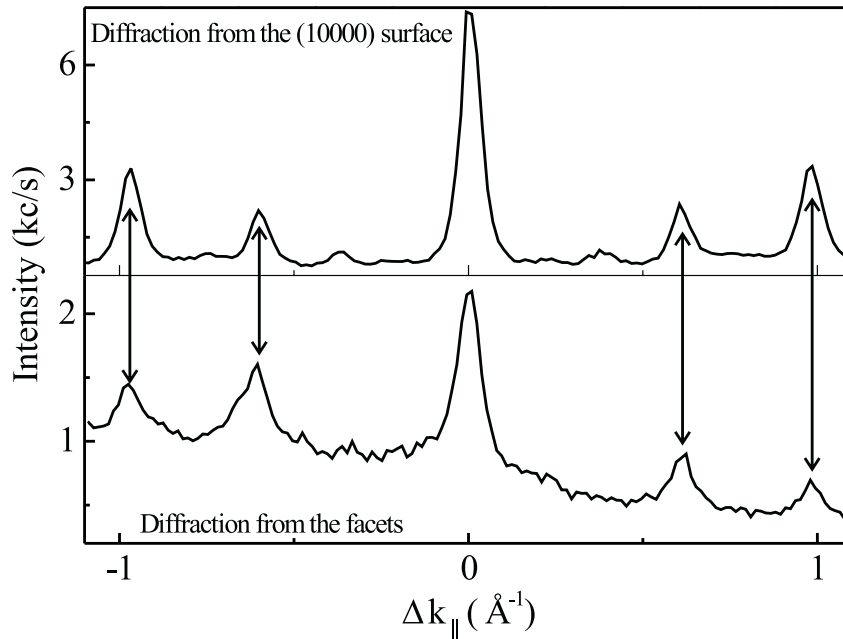


Figure 4.13: A comparison of He diffraction from the 2-fold (10000) surface along $[001\bar{1}0]$ (upper) and from the facets (lower).

and the 2-fold (10000) surface, their morphological features have been compared by measuring the specular intensity as a function of beam energy or momentum transfer. The variation of specular intensity with perpendicular momentum transfer reflects the vertical roughness of the surface (Section 3.2). Figure 4.14 shows the specular intensity variation for the facet plane and the 2-fold (10000) surface. The specular intensity varies in a similar fashion for both cases indicating the similar morphological feature of the facet planes and the 2-fold (10000) surface within a length equal to the transfer width of the instrument.

As the facets develop during normal surface preparation and do not have to be induced by a severe surface treatment, one likely explanation for the formation of the facets is a lower surface energy of the (10000) facet surface compared to that of the as-cut $(001\bar{1}0)$ surface. The shape of as-grown crystals supports the argument based on surface energy. The d -Al_{71.8}Ni_{14.8}Co_{13.4} single crystals grow as decagonal rods with growth faces of (10000)-orientation. Assuming the cross section parallel to the quasicrystalline plane reflects the equilibrium shape, this would indicate that the (10000) surface has indeed a lower surface energy than the $(001\bar{1}0)$ surface.

The size of the facets can be estimated from the FWHM of the facet specular peak, which is about 0.06 \AA^{-1} . It is limited by the instrumental resolution. Therefore, it is concluded that the

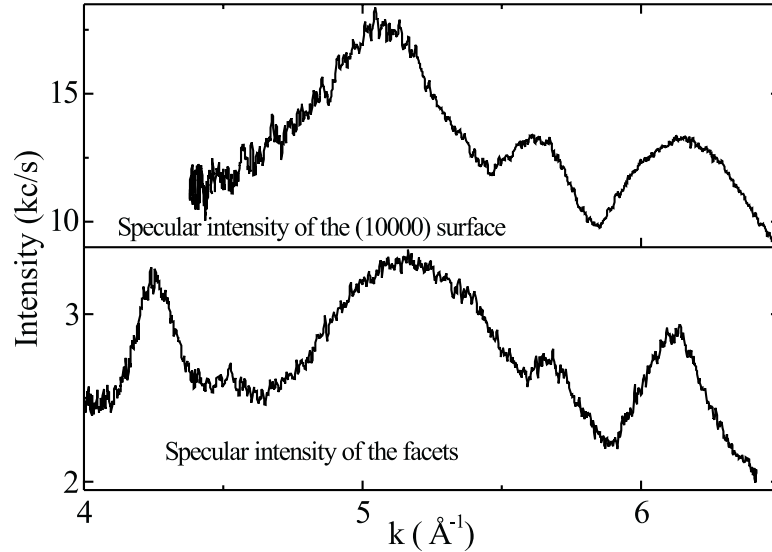


Figure 4.14: He specular intensity as a function of momentum transfer from the 2-fold (10000) surface (upper) and the facets (lower).

width of the facets along the quasiperiodic direction is in the order of 100 Å or larger. Similarly, the area covered by the facets can be calculated from the intensity of the main and facet specular peaks. The specular intensity of the as-cut surface is roughly twice the specular intensity of each of the facets inclined at either of $\pm 18^\circ$. The total specular intensity of the facets inclined in both directions is thus equal to the specular intensity of the as-cut surface. This shows that the faceted total area is approximately equal to the remaining non-faceted surface area.

Faceting is frequently observed in periodic systems and faceted surfaces are found to be technologically useful. They can be used to grow large-scale arrays of nanostructures, tilted superlattices, etc., because faceted surfaces exhibit selective adsorption planes [129]. Faceting in quasicrystals is very rarely observed. In fact, this is the first observation of faceting in quasicrystals with the exception of development of facets near the edge of a sample observed in 2-fold surface of i -Al-Pd-Mn [26].

The surface prepared by different sputtering and annealing conditions was investigated to learn the influences of preparation conditions on the developments of facets. The surface was sputtered at various temperatures varying from room temperature to around 800 °C (each step 10-30 minutes) and annealed up to 800 °C (10-30 minutes). Helium diffraction was recorded

after each sputter-annealing cycle (not shown here). All spectra are found to possess diffraction peaks related to facets. The profile of these peaks was not changed.

Summary

A very high corrugation of both 2-fold (10000) and (001 $\bar{1}$ 0) surfaces is inferred from the intensity distribution of the He diffraction. The observed SPA-LEED and HAS data reveal that the topmost surface layer retains a quasicrystalline order and the diffraction peaks are at positions expected from the bulk. The (10000) surface shows a hierarchy of diffraction spots, which can be explained on the basis of a 1D Fibonacci lattice.

As discussed, the (10000) and (001 $\bar{1}$ 0) surfaces have a common high symmetry direction along the 10-fold axis. The diffraction from both surfaces along the 10-fold axis shows the bulk expected 8 Å periodicity and a new periodicity of 16 Å. The intensity of the diffraction spots corresponding to the 16 Å periodicity is very weak and not particularly surface sensitive. This suggests that the 16 Å spots are related to the bulk and are not due to a surface reconstruction.

The (001 $\bar{1}$ 0) surface is found to develop facets of (10000)-equivalent orientation. The facet planes are identical to those observed in crystal growth, suggesting that their formation is due to a lower surface energy of the (10000)-compared to the as cut (001 $\bar{1}$ 0)-surface. The size of the facets is estimated to be 100 Å or larger. The area covered by the faceted planes is approximately 50 % of the total surface area. These results represent the first observation of facet formation in quasicrystals.